Hsa_circ_0053943 drives uveal melanoma progression via regulating N6-methyladenosine modification of EGFR with IGF2BP3

Andi Zhao
Jiangsu Province People's Hospital and Nanjing Medical University First Affiliated Hospital: Jiangsu Province Hospital and Nanjing Medical University First Affiliated Hospital

Yue Wang
Nanjing Medical University affiliated Nanjing Hospital: Nanjing First Hospital

Zijin Wang
Jiangsu Province People's Hospital and Nanjing Medical University First Affiliated Hospital: Jiangsu Province Hospital and Nanjing Medical University First Affiliated Hospital

Qing Shao
Jiangsu Province People's Hospital and Nanjing Medical University First Affiliated Hospital: Jiangsu Province Hospital and Nanjing Medical University First Affiliated Hospital

Qi Gong
Jiangsu Province People's Hospital and Nanjing Medical University First Affiliated Hospital: Jiangsu Province Hospital and Nanjing Medical University First Affiliated Hospital

Hui Zhu
Jiangsu Province People's Hospital and Nanjing Medical University First Affiliated Hospital: Jiangsu Province Hospital and Nanjing Medical University First Affiliated Hospital

Lei Liu
Jiangsu Province People's Hospital and Nanjing Medical University First Affiliated Hospital: Jiangsu Province Hospital and Nanjing Medical University First Affiliated Hospital

Xiaohan Zhang
Wuxi Children's Hospital

Shiya Shen
Jiangsu Province People's Hospital and Nanjing Medical University First Affiliated Hospital: Jiangsu Province Hospital and Nanjing Medical University First Affiliated Hospital

Hu Liu
Jiangsu Province People's Hospital and Nanjing Medical University First Affiliated Hospital: Jiangsu Province Hospital and Nanjing Medical University First Affiliated Hospital

Xuejuan Chen (✉ chenxuejuan@vip.163.com)
Jiangsu Province People's Hospital and Nanjing Medical University First Affiliated Hospital: Jiangsu Province Hospital and Nanjing Medical University First Affiliated Hospital

Research

Keywords: uveal melanoma, hsa_circ_0053943, IGF2BP3, EGFR, MAPK/ERK signaling pathway

Posted Date: June 23rd, 2022

DOI: https://doi.org/10.21203/rs.3.rs-1738662/v1

Abstract

Background

Increasing studies characterized the critical role of circular RNAs (circRNAs) as regulatory factors in the progression of multiple cancers. Nevertheless, the biological functions of circRNAs and their underlying molecular mechanisms in uveal melanoma (UM) progression remain enigmatic.

Methods

A novel circRNA, circ_0053943, was selected from re-mining UM microarray and quantitative RT-PCR. Functional assays were performed to investigate the roles of circ_0053943 in UM progression both in vitro and in vivo. To further explore the molecular mechanisms of circ_0053943 in UM, we implemented the fluorescence in situ hybridization, RNA pulldown assay, RNA binding protein immunoprecipitation assay, RNA sequencing, co-immunoprecipitation, and dual-luciferase reporter assays.

Results

Circ_0053943 was upregulated in UM and prompted the proliferation and metastatic ability of UM cells in vitro and in vivo. Mechanistically, circ_0053943 could bind to the KH1 and KH2 domains of insulin-like growth factor 2 mRNA-binding protein 3 (IGF2BP3), enhancing the function of IGF2BP3 by facilitating the stabilization of target mRNA. RNA sequencing assay identified epidermal growth factor receptor (EGFR) as a target gene of circ_0053943 and IGF2BP3 at the transcriptional level. Rescue assays revealed that circ_0053943 exerts its biologic function by stabilizing EGFR mRNA and regulating downstream the MAPK/ERK signaling pathway.

Conclusions

Circ_0053943 may promote UM progression by stabilizing EGFR mRNA and activating the MAPK/ERK signaling pathway through forming a circ_0053943/IGF2BP3/EGFR RNA-protein ternary complex, which in turn provide a potential biomarker and therapeutic target for UM.

Background

Uveal melanoma (UM) is the most common primary intraocular malignant tumor in adults, originating from melanocytes of the uveal tract, including iris, ciliary body, and choroid [1]. Despite aggressive management for the primary tumor, approximately 50% of patients will ultimately develop distant metastasis, particularly the liver, which leads to a poor prognosis within 5 months [2, 3]. Given such a poor long-term clinic outlook and the limitation of current treatments, there remains an unmet medical need to explore the mechanisms of UM tumorigenesis and evaluate novel effective therapies. Several

independent studies have identified an abundance of genetic aberrancies in UM, including mutations in *BAP1*, *SF3B1*, *EIF1AX*, and *Gα11/Q*, are involved and play essential roles in progression/metastasis [4, 5]. Nevertheless, the precise molecular mechanisms underlying UM remain primarily unclear.

Circular RNAs (circRNAs) comprise a recently discovered subclass of non-coding RNAs characterized by higher resistance to RNase R due to their closed continuous loop structures. This increased stability makes circRNAs more suitable for diagnostic biomarkers and therapeutic targets than other types of RNA [6]. Indeed, increasing evidence suggests that circRNAs are involved in metastasis and proliferation of multiple cancers through sponging microRNA (miRNA), interacting with RNA-binding proteins (RBPs), splicing pre-mRNA transcripts, and even encoding small peptides or proteins [7–9]. However, to date, a handful of published studies demonstrated circRNAs in UM, which is far fewer than the number of other cancers [10, 11]. Yang et al. published microarray data and screened out a list of differentially expressed circRNAs between UM and normal uveal tissues [10]. Based on these circRNAs, a further study indicated that upregulated circ_0119872, produced by host gene RAS guanyl releasing protein 3 (RasGRP3), could promote UM tumorigenesis via sponging miRNA and serve as an important prognostic biomarker [11]. Hence, to better understand the development and progression of UM, we explore novel insight into the role and mechanism of circRNAs in UM. Given that upregulated circRNAs can be more effectively used as therapeutic targets, we selected circ_0053943 for the subsequent in-depth study, also produced by the host gene *RasGRP3* and published in the top 10 overregulated circRNAs [10].

N6-methyladenosine (m^6A) is the most abundant epitranscriptomic modification of messenger RNAs (mRNAs), which contributes to the tumorigenesis of multiple cancers [12–14]. This modification is governed by methyltransferase complex ("writers"), demethylases ("erasers"), and RNA-binding proteins ("readers"). Insulin-like growth factor 2 mRNA-binding proteins (IGF2BPs; including IGF2BP1/2/3) is a newly identified class of distinct m^6A readers, facilitating m^6A-modified transcripts stability and translation [15, 16]. Recent studies have demonstrated that ncRNAs might participate in these IGF2BPs-mediated functions and modulate the expression of target transcripts [17–19]. Nonetheless, it remains to be elucidated the involvement of IGF2BPs in UM tumorigenesis and how underlying ncRNAs mediate these functional biological processes.

In the study, we identified a novel circRNA (hsa_circ_0053943) serving as an RNA m^6A reader-cooperator, assisting the m^6A reader (IGF2BP3) in guarding m^6A-modified EGFR against decay and promoting tumorigenesis and metastasis in UM. Our finding indicates that circ_0053943 may cooperate with IGF2BP3 in post-transcriptional regulation of EGFR and highlights the functional importance of the circ_0053943/IGF2BP3/EGFR mRNA-protein ternary complex in cell invasion and metastasis of UM cells.

Methods

Human tissue specimens

A total of 5 ocular melanoma tissues and 5 human normal melanocyte tissues were obtained from The First Affiliated Hospital of Nanjing medical university (Nanjing, China) from 2018 to 2021. The histological features of all specimens were evaluated by two experienced histopathologists independently. The clinicopathological characteristics of the UM patients are summarized in **Table S1**. Upon collection, all specimens were snap-frozen in liquid nitrogen and stored at − 80 °C until use. The study was approved by the Human Ethics Committee of First Affiliated Hospital of Nanjing Medical University, and each patient signed informed consent before the research started.

Cell culture

The human retinal pigment epithelial cell line (ARPE-19) and four ocular melanoma cell lines (MUM2B, C918, OCM-1, and OCM-1A) were purchased from the Cell Bank of Type Culture Collection of the Chinese Academy of Sciences (Shanghai, China). Human primary umbilical vein endothelial cells (HUVECs) were purchased from the American Type Culture Collection (ATCC, Manassas, VA). According to the manufacturers, all were cultured under recommended media and incubated at 37◦C in a moist incubator stabilized with 5% CO2. Cell lines used in this study were authenticated with short tandem repeat (STR) profiling.

RNA extraction and quantitative real-time polymerase chain reaction (qRT–PCR)

Total RNA of cell lines was extracted using TRIzol reagent (Invitrogen, CA, USA) and further reverse transcribed into cDNA using the PrimeScript RT Reagent Kit (Takara, Japan) according to the manufacturer's instructions. Subsequently, qRT-PCR using SYBR Green Kit (Takara, Japan) was performed on the StepOnePlus Real-Time PCR System (Applied Biosystems). The $^{-\Delta\Delta}C_T$ method was used to evaluate the transcript levels of mRNA. Either *GAPDH* or *U6* was used as an internal control. The sequences of primers used are listed in **Table S2**.

Transfection

Recombinant lentivirus containing short hairpin RNA targeting circ_0053943 (sh-circ_0053943#1/2/3) and IGF2BP3 (sh-IGF2BP3#1/2), along with full-length targeting sequence of circ_0053943 and IGF2BP3, including the corresponding negative control, were synthesized by RiboBio (Guangzhou, China). The IGF2BP3 full length (FL) and truncation-mutation plasmids with a C-terminus 3× Flag tag were synthesized by Obio (Shanghai, China). The small interfering RNA (siRNA) oligonucleotides targeting METTL3 and METTL14 were synthesized by RiboBio (Guangzhou, China). Lipofectamine 3000 (Invitrogen) was used to transfigure shRNAs and plasmid vectors. The transfection efficiency was confirmed through qRT-PCR. Detailed sequences of shRNAs and siRNAs are provided in **Table S3**.

Cell proliferation assay and Flow cytometry assay

Cell proliferation/growth was assessed by Cell Counting Kit8 (CCK-8) using the commercial CCK-8 kit (Dojindo Laboratories, Dojindo, Japan) and 5-ethynyl-2 -deoxyuridine (EDU) assay using the Cell-Light

EdU Apollo 488 In Vitro Kit (RiboBio, Guangzhou, China.), according to the manufacturer's protocols.

For the Cell cycle assay, the treated cells were fixed in 75 % alcohol overnight at -20 °C. After being washed three times, the fixed cells were stained with propidium iodide (PI) buffer using a Cell Cycle Analysis Kit (Beyotime, Shanghai, China). All treated cells were incubated with H2O2 (1 mM) for 4 h to stimulate apoptosis for cell apoptosis assays. Then the cells were stained with Annexin VAPC/7-AAD Apoptosis Detection Kit (KeyGEN, Jiangsu, China) according to the manufacturer's protocol. Finally, both the cell cycle distribution percentage and Apoptotic rates were determined by flow cytometry (CytoFLEX; Beckman Coulter, Inc.) and analyzed with Flowjo 7.6.1 software.

Cell migration and invasion assays

Transwell assay was performed to evaluate the abilities of cell migration and invasion using Transwell chambers (Corning Life Sciences, MA, USA). Briefly for migration assay, 2×10^4 transfected UM cells were suspended in a 200 μl serum-free medium in the upper chamber, while the lower chamber was filled with an 800 μl medium containing 10% FBS. After 24 h or 48 h (based on different cell lines), the upper chamber was washed, fixed, stained by 0.25% crystal violet, and counted under a light microscope. The cell numbers were counted in 3 random fields of view. For invasion assay, the same steps were performed as those for the migration assay described above except that Matrigel (BD Biosciences, Franklin Lakes, NJ, USA) was pre-coated onto the upper layer for 60 min at room temperature before the experiment.

For wound healing assay, a 200-μL pipette tip was used to perform a vertical scratch wound in the middle slide after cells transfected and seeded at least 90% fusion into 6-well plates. Pictures of the wound were taken at the same position under a microscope at 0 and 24h. Migration ability was analyzed by quantitatively evaluating the gap distance using ImageJ software.

Fluorescence in situ hybridization and immunofluorescence

RNA fluorescence in situ hybridization (FISH) was performed to detect the subcellular localization of circ_0053943 in MUM2B, C918, and OCM-1A cells, by using a FISH Kit (RiboBio, Guangzhou, China) following the manufacturer's directions. Circ_0053943-specific Cy3-labeled probes were designed and synthesized by RiboBio (Guangzhou, China). Briefly, after being fixed with 4% paraformaldehyde, permeabilized with 0.5% Triton X-100 (PBS), and blocked with prehybridization buffer, the cells were incubated in a hybridization buffer containing FISH probe overnight. Then The cells were rinsed with sodium citrate buffer and incubated with Hoechest 33342 (ThermoFisher Scientific, MA, USA) for nuclear staining. For dual RNA-FISH and immunofluorescence, the cells were blocked with an immunostaining blocking solution (Beyotime, Shanghai, China) after incubation with the hybridization buffer containing the FISH probe. Subsequently, cells were incubated with primary antibodies overnight and labeled with fluorescence-conjugated secondary antibody for 1 h in the dark. After incubation, Hoechest 33342 (ThermoFisher Scientific, MA, USA) was added to each sample for nuclear visualization. Finally, images were obtained using Nikon A1Si Laser Scanning Confocal Microscope (Nikon Instruments Inc., Japan).

Western blotting (WB)

Tissue or cellular protein was lysed in RIPA lysis buffer (Beyotime, Shanghai, China) following the instructions, and the protein concentration was detected by the BCA kit (Vazyme, Nanjing, China). Western blotting (WB) experiments and quantification of the signals were performed according to the manufacturer's protocols. The antibody information is shown in **Table S4**.

RNA pulldown assay

The biotin-labeled pulldown probe targeting circ_0053943 and negative control were designed and synthesized by Ribobio (Guangzhou, China), details shown in **Table S5**. The RNA-pulldown assay was performed with the Pierce Magnetic RNA-Protein Pull-Down Kit according to the protocol (ThermoFisher Scientific, MA, USA). Briefly, lysates from UVM cells were incubated with transcribed biotin-labeled circ_0053943 and pulled down with streptavidin beads. The eluted proteins from the RNA pulldown assay were subjected to mass spectrometric analysis or western blot. The list of RNA-binding proteins (RBPs) identified by mass spectrometry is shown in **Table S6**.

Luciferase reporter assay

Luciferase reporter assay was performed according to the manufacture's protocol.

RNA sequencing

RNA-seq libraries were constructed in circ_0053943 silenced MUM2B cells. Firstly, RNA Integrity was checked by Agilent 2100 Bioanalyzer (Genesky, Shanghai, China) after quality inspection with starting RNA at 2 μg. Secondly, Oligo-dT magnetic bead was used for mRNA purification and fragmentation to 100-300 bp. Thirdly, first- and second-strand cDNA was synthesized**,** followed by end repair and adenylate 3' ends. Finally**,** after ligating adapters, fragments size selection**,** and PCR amplification, a HiSeq system (Illumina, San Diego, CA, USA) on Pair End was used for RNA high-throughput sequencing.

RNA immunoprecipitation (RIP)

A RIP Kit (Millipore, Burlington, MA, USA) was purchased for RNA immunoprecipitation assays. Firstly, cells were lysed by RIP lysis buffer, along with protease and RNase inhibitors. Secondly, the magnetic beads were mixed with 10 μg anti-IGF2BP3, anti-Flag, or anti-IgG antibodies. Then, cell lysates were mixed with magnetic beads and antibodies at 4 ℃ overnight. Finally, the immunoprecipitated RNA was extracted for qRT-PCR after RNA purification.

RNA stability assay

Relevant RNA expression was measured by qRT-PCR after the extracted RNA of UM cells was incubated with or without RnaseR (3 U/μg) for 10min at 37 °C. For actinomycin D treatment, theTotal RNA of UM cells was harvested every six hours after the treatment (5 μg/ml). Then the variation trends of circ_0053943 and *RasGRP3* were detected by qRT-PCR.

Animal model

10^6 transfected cells were resuspended in PBS and subcutaneously injected into the armpits of BALB/c nude mice (four weeks old, male), purchased from the Animal Center of Nanjing medical university (Nanjing, China) for xenograft model. The volume of tumors was calculated every week. All the mice were sacrificed after 4 weeks. Tumors were resected and fixed in formalin for following Immunohistochemistry detection.

For tumor metastasis assay in vivo, 10^6 relevant cells resuspended in 50 μl PBS were injected into the mice spleen via the left epigastric incision. The livers of mice were resected and fixed after six weeks. All the animal experiments were performed according to the institutional and guidelines of the Committee on the Ethics of Animal Experiments of Nanjing Medical University.

Statistical Analysis

Every experiment was repeated at least three times. SPSS 13.0 software (Chicago, IL, USA) and GraphPad Prism software (La Jolla, CA, USA) was used for the statistical analyses. The variation analysis of two groups was performed with Student's t-test, while ANOVA was used to analyze the difference among more than two groups.

Results

Circ_0053943 is upregulated in UM tissues

In the present study, we focused on upregulated circRNAs based on the published circRNA microarray data between UM and normal uveal tissues (**Fig. S1A**) [10]. Therefore, the qRT-PCR was performed to detect these upregulated circRNAs in 5 UM and normal tissues for further validation. Hsa_circ_0053943 was prominently overexpressed in UM tissues compared to normal group (**Fig. 1A**), similar to hsa_circ_0119872 reported previously (**Fig. S1B**) [10, 11]. Then, we detected the expression level of circ_0053943 in UM cell lines; as shown in **Fig. 1B**, its expression in ARPE-19 cells was significantly lower than that in UM cell lines. Thus, the uncharacterized hsa_circ_0053943 was chosen for our subsequent in-depth study.

Hsa_circ_0053942 (cric_0053943) is generated from exons 9, 10, and 11 of the *RasGRP3* gene and is 567 nucleotides in length according to the circBase annotation (**Fig. 1C**) [20]. To validate the back-splice junction site of circ_0053943, we performed a series of experiments, including PCR amplification, agarose gel electrophoresis, and Sanger sequencing. Subsequently, convergent and divergent primers were designed to amplify the linear and back-splicing products based on cDNA and genomic DNA (gDNA) from UM cells. The subsequent agarose gel electrophoresis demonstrated that the convergent primers could amplify products of expected size from cDNA and gDNA, both for circ_0053943 and GAPDH. However, divergent primers for circ_0053943 could only amplify a PCR product from cDNA but not from gDNA. Meanwhile, no product was observed after being amplified by divergent primers for GAPDH in cDNA or

gDNA (**Fig. 1D**). We next conducted an RNase R treatment assay to confirm the circular characteristics of circ_0053943 further. The results demonstrated that circ_0053943 was more resistant to RNase R and actinomycin D treatment than linear RasGRP3 mRNA **(Fig. 1E** and **Fig. S1C**). In addition, subcellular fractionation assays, including RNA-FISH and RNA nucleus/cytoplasm separation, revealed that circ_0053943 was predominantly localized in the cytoplasm (**Fig. 1F, G**). These data suggested that circ_0053943 was a circular structure and upregulated in a large portion of UM, which might serve as a prognostic biomarker.

Circ_0053943 promoted the proliferation and metastasis of UM cells

Three shRNAs targeting circ_0053943 were transfected into MUM2B and C918 cells to elucidate the biological role of circ_053943 in UM proliferation and metastasis, according to the comparatively high expression in these two cell lines. Meanwhile, OCM-1 and OCM-1A cells were stably developed with a circ_0053943 overexpression lentivirus. At the same time, the expression of RasGRP mRNA remained unchangeable in either circ_0053943 knockdown or stable overexpressing cells. Further, shRNA#1 and #2, and a scrambled non-target shRNA control, were chosen for the subsequent cell phenotype assays, considering their greater knockdown efficiency (**Fig.S1D, E**).

The growth curves performed by CCK8 assays were suppressed significantly by down-regulated circ_0053943 (**Fig. 2A**), whereas upregulated circ_0053943 prominently promoted OCM-1 and OCM-1A cells (**Fig. 2B**). Similarly, the EDU staining assay confirmed that the number of EDU-positive MUM2B and C918 cells (proliferative cells), following transfected with shRNAs, was decreased compared with the control group (**Fig. 2C**). Conversely, the OCM-1 and OCM-1A cells transfected with overexpressed lentivirus revealed a significant increase compared with the control group (**Fig. 2D**). Transwell assays and scratch wound healing assays revealed that circ_0053943 knockdown led to a significant decrease in cell migration and invasion ability in MUM2B and C918 cells. In contrast, circ_0053943 overexpression increased the ability of OCM-1 and OCM-1A cells (**Fig. 2E-I**).

The flow cytometric assays of cell cycle distribution indicated that downregulating circ_0053943 increased the percentage of G0/G1 phase and decreased S phase populations in MUM2B and C918 cells, compared with the control group (**Fig. 3A**). Conversely, the overexpression of circ_0053943 induced the progression of G1-to-S phase transformation and suppressed apoptosis remarkably in OCM-1 and OCM-1A cells (**Fig. 3B**). Apoptosis assay showed that cells transfected with shRNAs had higher apoptotic rates than the control group, while transfection of overexpressed lentivirus decreased the apoptotic cells (**Fig. 3C, D**). In addition, Cyclin D1/CDK4 was reported to induce G1/S transition, while Bcl-2 (anti-apoptotic protein) /Bax (pro-apoptotic protein) was described to regulate cell apoptosis antagonistically. Thus, western blot was used to determine critical molecules involved in the cell cycle and apoptosis. Results demonstrated that when knocking down circ_0053943, the protein expression levels of Cyclin D1, CDK4, Bcl-2, and Bax were reduced or increased in a manner consistent with the results of the flow cytometric assays while overexpressing circ_0053943 had the opposite effects (**Fig. 3E**).

The abovementioned findings indicated that circ_0053943 might behave as an oncogene by promoting proliferation, metastasis, and invasion in UM cells.

Circ_0053943 and IGF2BP3 cooperate to play oncogenic roles

Given that circRNAs can influence the bio functions via sponging miRNAs, a RIP assay was conducted to test if circ_0053943 regulates targets as a miRNA sponge in UM. Interestingly, the results showed that the AGO2 antibody significantly enriched ciRS-7 (a circRNA binding with AGO2), but not circ_0053943 (**Fig. S2A**), suggesting circ_0053943 may not act as a miRNA sponge in UM progression.

Then we conducted an RNA pulldown assay coupled with mass spectrometry (MS) to explore whether circ_0053943 exerted function via interacting with proteins (**Fig. S2B**). The MS assay revealed 167 differential proteins between the sense and antisense circ_0053943 transcript pulldown groups in MUM2B cells (**Table S6**). Afterward, overlapped differential proteins with RBPs (**Table S7**) and 50 proteins were found to be potential partners. Since circ_0053943 was mainly localized in the cytoplasm, cytoplasmic protein could interact with circ_0053943. Biotin-labeled RNA pulldown assay and separated by SDS-PAGE were performed with cytoplasmic protein in MUM2B cells. After silver staining, the sense-specific band at about 55-70 kDa was excised (**Fig. 4A**). Among the 50 differential proteins, 3 proteins might be potential protein partners of circ_0053943. Notably, only IGF2BP3 could be detected in the input group and circ_0053943 pulldown products but not in the antisense pulldown products (**Fig. 4B** and **Fig. S2C**). Furthermore, Kaplan-Meier survival analysis in TCGA cohorts showed that the patients with higher IGF2BP3 expression were associated with shorter overall survival (OS) and disease-free survival (DFS) rates (**Fig. 4C**).

As shown in **Fig. 4D** and **Fig. S2D**, the anti-IGF2BP3 antibody could specifically enrich circ_0053943 compared with the anti-IgG antibody following the RIP assay results. In addition, the Dual RNA-FISH and immunofluorescence assay showed the co-localization of circ_0053943 and IGF2BP3 in MUM2B and C918 cells, thereby further supporting their interaction (**Fig. 4E**). Then, to determine which domain is interacted with circ_0053943, we designed 6 truncated IGF2BP3 plasmids aiming at 6 functional domains. Protein domain mapping and RIP assay showed that the KH1 and KH2 domains were essential for the interaction between IGF2BP3 and circ_0053943 (**Fig. 4F-H**). Overexpression or knockdown of circ_0053943 could not affect the mRNA and protein levels of IGF2BP3 (**Fig. 4I** and **Fig. S2D, E**), while no significant changes in the expression of circ_0053943 were also observed after IGF2BP3 was knocked down (**Fig. 4J** and **Fig. S2F**). Of note, IGF2BP3 depletion could abolish the induction of cell proliferation, migration, and invasion elicited by the circ_0053943 overexpression. In contrast, IGF2BP3 overexpression could not affect the proliferation and metastatic ability of UM cells while circ_0053943 was simultaneously knocked down (**Fig. S3A-F**). Collectively, these results suggest that circ_0053943 and IGF2BP3 may cooperate to play oncogenic roles in UM cells.

EGFR was identified as a downstream target of circ_0053943 and IGF2BP3

Given that circ_0053943 specifically interacts with IGF2BP3 but does not affect the protein levels, we next investigated how circ_0053943 promoted UM progression through IGF2BP3. Previous studies reported that IGF2BP3, which stabilized an extensive repertoire of target mRNA transcripts, was dysregulated and played an oncogenic role in diverse types of cancers [21-22]. To confirm this hypothesis, RNA-sequence was used to profile the global effects of circ knockdown compared with the negative control in MUM2B cells. Gene expression profiling after circ_0053943 knockdown showed a total of 4,293 genes with expression changes, including 2,308 upregulated genes and 1,985 downregulated genes (**Fig. 5A**). Furthermore, pathway enrichment analysis based on the Kyoto Encyclopedia of Genes and Genomes (KEGG) database showed the top 12 signaling pathways where the MAPK pathway was most enriched (**Fig. 5B**). Considering the MAPK signaling pathway was identified by KEGG pathway enrichment analysis, the critical components of the MAPK pathway, p38, ERK, JNK, and their corresponding phosphorylation forms were evaluated using western blot. As displayed in **Fig. 5C**, the levels of P38, ERK1/2, and JNK did not show significant changes after silencing the circ_0053943. Meanwhile, the phosphorylated forms of these proteins were reduced, and the reduction in phosphorylated ERK showed the most significance. These findings indicated that circ_0053943 might promote UM proliferation and metastasis by regulating the MAPK/ERK signaling pathway.

To this end, we performed an integrated analysis among our RNA-sequence data, two published IGF2BP3 RIP-sequence data [18], and critical components in the MAPK signaling pathway to define the target genes potentially regulated by circ_0053943 and IGF2BP3. Among 1,985 downregulated genes via depletion of circ_0053943, 1,159 genes had IGF2BP3's enrichment on their transcripts through two independent IGF2BP3 RIP-sequence data, and 25 genes act as possible key targets in the MAPK signaling pathway (**Fig. 5D**). Strikingly, survival analysis was performed based on the expression status of these 25 genes by GEPIA 2 [23], and 10 genes showed prognostic impacts in UM (**Fig. 5E** and **Fig. S4A, B**). We then selected these 10 genes as possible targets for further validation in circ_0053943 and IGF2BP3 knockdown cells. Similar to the RNA-seq results, the transcript levels of *ARRB2*, *EGFR*, *FGFR4*, *PDGFA*, and *PDGFB* were decreased via depletion of circ_0053943, while only EGFR was showed a significant decrease of more than 50% both in circ_0053943 depletion and IGF2BP3 depletion cells (**Fig. 5F**).

Thus, EGFR was chosen as the IGF2BP3-bound target altered by circ_0053943 for further research. Western blot analysis confirmed that knockdown of either circ_0053943 or IGF2BP3 reduced the protein levels of EGFR (**Fig. S5A**). In addition, q-PCR and western blot showed that knocking down circ_0053943 abrogated the long-lasting effect of IGF2BP3 overexpression on the EGFR transcript. Conversely, reducing IGF2BP3 abolished the half-life and mRNA level of increased by circ_0053943 overexpression (**Fig. 5G, H** and **Fig. S5B, C**). Collectively, these data suggest a functional interdependency between circ_0053943 and IGF2BP3 when stabilizing the EGFR transcript.

Circ_0053943 cooperates with IGF2BP3 to stabilize EGFR mRNA in an m^6A-dependent manner

Considering that IGF2BPs (including IGF2BP1/2/3) was characterized as a new m^6A reader that regulates mRNA of m^6A-modified genes (such as MYC), we hypothesize that circ_0053943 and IGF2BP3 might

regulate the stability of EGFR mRNA in an m^{6}A-dependent manner. To confirm this hypothesis, we first identified the potential m^{6}A-modified regions of EGFR based on the m^{6}A RIP-sequence data. Through analyzing the m^{6}A-RIP sequencing data, we detected several significant m^{6}A peaks that were markedly reduced by knockdown of m^{6}A “writers” silencing (i.e., methyltransferase-like 3 and 14 (METTL3 and METTL14)), in 5’- and 3'-untranslated regions (3’UTR and 5’UTR) of EGFR mRNA (**Fig. 6A**). Moreover, enrichments of the canonical “GGAC” m^{6}A motif in these m^{6}A peaks confirmed our hypothesis that EGFR mRNA is modified by m^{6}A methylation.

Next, we performed m^{6}A-specific RIP, followed qRT-PCR assay to determine the m^{6}A methylation level of EGFR in METTL3 and METTL14 knockdown cells (**Fig. S6A**). The result showed that the m^{6}A methylation of the 3’UTR, but not the 5’UTR of the EGFR transcript, was substantially decreased. In line with a previous study, the coding region instability determinant (CRD) of MYC (positive control) was also reduced. However, the negative control of HPRT1 did not show a similar reduction, which confirmed that EGFR was modified by m^{6}A (**Fig. 6B**). Due to IGF2BP3 being early proven to preferentially bind to the “GGAC” m^{6}A core motif of its targets [18], we further checked whether circ_0053943 affects IGF2BP3 binding the m^{6}A-modified EGFR. The IGF2BP3 RIP qRT-PCR assays showed that knockdown of circ_0053943 significantly reduced IGF2BP3 binding to the m^{6}A site in the 3’UTR region of EGFR, and the overexpression of circ_0053943 facilitated this binding, but not in the EGFR 5’UTR or MYC CRD (**Fig. 6C**). These results further indicated that circ_0053943 specifically enhances the occupancy of IGF2BP3 at 3’UTR of EGFR. Moreover, using RNA pulldown assay with in vitro-transcribed circ_0053943, we found that the binding abilities of circ_0053943 to the 3’UTR of EGFR were nearly abolished following IGF2BP3 knockdown and increased after IGF2BP3 overexpressed (**Fig. S6B**). Thus, it confirmed that circ_0053943 might bind the 3’UTR of EGFR in an IGF2BP3-dependent manner.

In the 3’UTR region of EGFR, we preliminarily found 2 “GGAC” m^{6}A motifs predicted by m^{6}A modification site predictors SRAMPA (http://www.cuilab.cn/sramp) and RMBase V2.0 (http://rna.sysu.edu.cn/rmbase/index.php) (**Fig. 6D**). Subsequently, we constructed luciferase reporters that contain the wild-type EGFR 3'UTR (WT-3’UTR), mutant #1 and #2 3'UTR (Mut#1- and Mut#2-3’UTR; changing GGAC to GGCC), to elucidate the potential roles of circ_0053943 in m^{6}A modification of EGFR (**Fig. 6E**). Compared to the Mut#2-3’UTR reporter, both IGF2BP3 and m^{6}A RIP qRT-PCR assays showed higher enrichment with the WT and Mut#1-3’UTR reporters. Additionally, overexpression of circ_0054943 or IGF2BP3 remarkably increased the binding of IGF2BP3 and m^{6}A in the WT and Mut#1-3’UTR reporters, but not in the Mut#2-3’UTR report. Conversely, knocking down circ_0053943 and IGF2BP3 independently reduced this binding except in the Mut#2-3’UTR report (**Fig. 6F, G**). Furthermore, luciferase reporter assays demonstrated that the relative luciferase activities were decreased by knockdown circ_0053943 or IGF2BP3 in WT and Mut#1-3’UTR reporters, but not in Mut#2-3’UTR reporter. Similarly, the relative luciferase activity of MUT#2-3’UTR reporter was also not altered by overexpressed circ_0054943 or IGF2BP3 (**Fig. 6H, I**). Thus, methylation of m^{6}A-modified site c.4510A in the 3’UTR of EGFR mRNA contributed to the EGFR expression.

Collectively, these data revealed that circ_0053943 cooperates with IGF2BP3 to increase EGFR mRNA stability in an m^6A-dependent manner and further indicated that circ_0053943 might strengthen the m^6A recognition by IGF2BP3 and recruitment of RNA stabilizers to m^6A-methylated EGFR mRNA.

Circ_0053943 promoted UM proliferation, metastasis, and angiogenesis through upregulating EGFR in vitro

Given that circ_0053943 could promote the proliferation and metastasis of UM and the expression of EGFR, we hypothesized that circ_0053943 might promote UM progression by inducing EGFR expression. Hence, we developed an EGFR-specific shRNA(sh-EGFR) with negative control (sh-Ctrl) to suppress the expression of EGFR and an overexpression plasmid to upregulate the expression in UM cells. Transfection efficiency was examined at the mRNA levels and displayed in **Fig. S7A**.

As shown in cell proliferation assays, EGFR silencing could remarkably inhibit the proliferation ability of circ_0053943 overexpression cells. In contrast, EGFR overexpression could promote UM cell proliferation ability of circ_0053943 knockdown cells (**Fig. 7A, B** and **Fig. S7B, C**). Transwell assays indicated that metastasis abilities in sh-EGFR cells were significantly increased compared to those in sh-Ctrl cells when circ_0053943 was silenced (**Fig. 7C** and **Fig. S7D**). Similar results were also observed in the wound healing assay (**Fig. 7D** and **Fig. S7E**).

In addition to cell division, increased motility, and decreased apoptosis, EGFR expression was described to play an essential role in tumor angiogenesis. Given these findings, we analyzed the potential implication of the circ_0053943/IGF2BP3/EGFR mRNA-protein ternary complex on angiogenesis using HUVEC tube formation assay. As depicted in **Fig. S7F**, conditioned medium (CM) from sh-circ_0053943 MUM2B cells reduced the formation of capillary-like structures by HUVECs dramatically compared to control conditioned medium. In contrast, EGFR overexpression reversed the capillary-like structure formation decreased by circ_0053943 depletion. In contrast, CM from circ_0053943 OCM-1A cells showed the promoting effects on the formation of capillary-like structures, which were inhibited by silencing EGFR as shown in **Fig. S7G**. Together, these results demonstrated that overexpression of circ_0053943 increased capillary-like structure formation in HUVECs by regulating EGFR expression.

To this end, the expression of cycle-related proteins (Cyclin D1, CDK4) and apoptosis-related proteins (Bcl-2, Bax) were measured by performing western blotting. The results showed that the knockdown of circ_0053943 impaired the G1 to S translation by downregulating CDK4 and Cyclin D1, and the overexpression of EGFR could rescue this effect. The overexpression of circ_0053943 could promote the G1 to S transition, while silencing EGFR could impair this translation. On the other hand, the alterations of Bcl2 and Bax demonstrated that the anti-apoptotic effect of circ_0053943 could be weakened by the knockdown of EGFR (**Fig. 7E, F**).

Taken together, all the above demonstrated that increased circ_0053943 might upregulate the expression of EGFR, which further promotes UM proliferation and metastasis.

Circ_0053943 promoted UM proliferation and metastasis through upregulating EGFR in vivo

To investigate the effects of circ_0053943 on UM proliferation and metastasis in vivo, we next established subcutaneous xenograft nude mice models. MUM2B and OCM-1A cells transfected with sh-circ_0053943/sh-EFGR/overexpression plasmids, along with relative control group and co-transfection group, were separately injected into nude mice. As shown, tumor growth was repressed by circ_0053943 knockdown, with lesser tumor volume and weight than control groups, while overexpression of EGFR could reverse the growth inhibition caused by circ_0053943 depletion (**Fig. 8A, B**). In OCM-1A cells, circ_0053943 overexpression had an opposite effect, which was repressed by EGFR depletion (**Fig. 8C, D**). Additionally, the results of IHC showed that Ki-67 (the marker for tumor proliferation) and EGFR expression levels were decreased in the circ_0053943 depletion group and increased in the overexpression group (**Fig. 8E**).

Next, we investigated the effect of circ_0053943 on tumor metastasis in vivo. The anatomical results confirmed that the metastatic nodules were lessened in the circ_0053943 knockdown group compared with the control group. In contrast, the metastatic lesions at the liver surface were more abundant in the EGFR overexpression group. Further analysis showed that the reduction of metastatic nodules caused by circ_0053943 depletions was increased by EGFR overexpression. In contrast, the opposite effect was obtained in nude mice injected with circ_0053943/sh-EGFR cells (**Fig. 8F-H**).

Taken together, the results of the in vivo experiments strongly suggested that circ_0053943 upregulation enhanced the proliferation and metastatic capacity of UM by upregulating EGFR in vivo.

Discussion

The current study demonstrated a vital circRNA circ_0054943, highly expressed in UM cells, acting as an oncogene in UM. Our phenotype experiment reveals that circ_0053943 promotes proliferation, migration and invasion, and angiogenesis of UM cell lines in vitro. The patient-derived xenograft UM model further validated its effect on tumorigenesis and hepatic metastasis in vivo. Our study first identified that circ_0053943 promotes UM progression via a new regulatory mechanism by interacting with protein. In detail, increased expression of circ_0053943 cooperates with IGF2BP3 forming a circ_0053943/IGF2BP3/EGFR mRNA-protein ternary complex. This formed mRNA-protein ternary complex consequently enhances the stability of EGFR mRNA, which leads to upregulation of EGFR and then activates MAPK/ERK signaling pathways in UM (Fig. 9).

Although UM is a relatively rare subtype of melanoma, it was previously found to share minimal overlapping genetic signatures with cutaneous melanoma [5, 24, 25]. In UM, genetic aberrancies are believed to be the driver of tumor carcinogenesis through abnormal activation of the Gα11/Q pathway [26, 27]. In particular, genes including *GNAQ*, *GNA11*, *PLCB4*, and *CYSTLR2*, and three secondary driver genes (*BAP1*, *SF3B1*, *EIF1AX*), have been reported to frequently mutated in a substantial fraction of UM tissues [26, 28–30]. Even so, somatic mutations above were only observed in a limited number of UM tumors, and *GNAQ* and *GNA11* are relatively weak oncoproteins without co-mutated secondary driver

genes [31]. Prior studies have noted the importance of aberrant ncRNA expressions in oncogenesis, which provides a unique opportunity to optimize treatment paradigms and establish new therapeutic options for UM [32–35]. Therefore, further studies on the pathological functions of ncRNA are required to obtain a complete picture of the undeveloped regulatory mechanisms under these somatic mutations.

CircRNAs are novel endogenous ncRNAs that form a covalently closed loop structure. Growing evidence indicates that dysregulated circRNA was associated with clinic pathologic features in various tumors, confirming its latent biological functions [36, 37]. So far, there were only two studies involving dysregulation of circRNAs in UM. Yang et al. screened out the abnormal expression profile of circRNAs in UM tissues but did not investigate the mechanisms [10]. Based on these published circRNAs, Liu et al. indicated that upregulated cytoplasmic circ_0119872 could promote UM tumorigenesis via sponging miRNA and modulating the activity of miRNAs on the target genes [12]. Even though circ_0053943 was also predominantly located in the cytoplasm of UM cells, it was accidentally found unable to bind with AGO2, thus excluding the possibility of it being a miRNA sponge. Up to date, other mechanisms of circRNAs in tumor progression, especially in UM, have not been thoroughly explored. Herein, we identified a novel circRNA, circ_0053943, interacting with KH1 and KH2 domains of IGF2BP3 and enhancing its biological function.

IGF2BPs (IGF2BP1, IGF2BP2, and IGF2BP3) are a newly discovered family of m^6A "reader," while m^6A is recognized as an abundant post-transcriptional modification and regulated mRNAs stability and translation [38, 39]. Although a handful of findings have demonstrated the critical role of m^6A modification in UM tumorigenesis, little is known about the effects of the newly discovered reader, IGF2BPs, in UM [40, 41]. Wan et al. reported that the transcription of IGF2BP3 is widely upregulated in multiple ocular cancers, including UM [42]. The survival analysis using TCGA further indicates that IGF2BP3 can act as an independent predictor for prognosis in UM. Our finding proposes a latent mechanism by which IGF2BP3 facilitates the tumor's development and supports that circ_0053943 enhances this function in UM. Mechanistically, under the control of circ_0053943, IGF2BP3 is directly bound to the m^6A site and formed circ_0053943/IGF2BP3/EGFR mRNA-protein ternary complex, which enhances mRNA stability or translation of EGFR in an m^6A manner. However, the molecular mechanism of IGF2BP3 overexpression in the UM remains enigmatic.

EGFR, a 170-kDa transmembrane tyrosine kinase receptor, is detected in a wide variety of malignant cells and has been reported to play a vital role in tumor development and progression [43]. Additionally, EGFR has been reported to regulate various downstream signaling pathways, including phosphatidylinositol-3-kinases/protein kinase B (PI3K/Akt) and mitogen-activated protein kinase/extracellular regulated protein kinases (MAPK/ERK) signaling pathways [44–47]. Accumulating evidence shows that enhanced EGFR expression is significantly associated with tumor development and suggests an indicator of poor prognosis in UM [48, 49]. Whereas, most of these studies only focused on verifying overexpressed EGFR affects cancer cell proliferation and migration, which is only part of the story since the cause of EGFR overexpression in UM has not been investigated. Therefore, we proved that overexpressed circ_0053943 could upregulate the EGFR expression through the circ_0053943/IGF2BP3/EGFR complex and activate

the MAPK/ERK pathway. These findings were consistent with a previous study [50] and offered possible upstream regulators.

Our study provides evidence that the action of circ_0053943 and IGF2BP3 in regulating the m^6A-modification of EGFR cooperatively in UM. To our knowledge, this is the first report that shed new light on post-transcriptional EGFR expression, providing an essential role for circRNAs in RNA metabolism. However, the mechanisms that upregulate circ_0053943 and mediate the export of circ_0053943 from the nucleus to the cytoplasm need further study. Besides, we did not determine how circ_0053943 mediated the interaction between IGF2BP3 and EGFR by specifically binding to the KH1 and KH2 domains IGF2BP3. RNA-seq and the subsequent qRT-PCR verify that the function of circ_0053943 on IGF2BP3-modified target mRNA is selective. This specificity of ncRNA function remains elusive but is in line with a recent study based on ccRCC. The study showed that *DMDRMR* could also enhance the IGF2BP3-mediated m^6A modification of the target genes by interacting with the KH1 and KH2 domains [51]. Thus, we believe that some correlation might exist between the two studies. Finally, there is no denying that the published IGF2BP3 RIP-sequence data mentioned in this study are not from UM cell lines [18]. Hence, the identification of IGF2BP3 binding molecular spectrum based on UM cells needs to be further explored in the future.

Another unique strength of our study is that we substantiated our results by using an in vivo metastasis animal model. We identified that high expression of circ_0053943 in UM cells dramatically promoted proliferation, migration, and angiogenesis in the animal model. Despite that these animal models may not reproduce the complexity of UM in human beings, our findings from this animal model partly support the clinic data and in vitro function of circ_0053943 in promoting UM development. To date, MAPK/ERK kinase (MEK) inhibitors in the management of metastatic uveal melanoma management are still controversial, considering inevitable side effects [51, 52]. Our findings indicate that circ_0053943 might potentially act as a novel therapy target for UM.

Conclusions

In summary, we identified a novel circRNA, has_circ_0053943, overexpressed in UM and associated with a poor prognosis. Upregulating circ_0053943 exerted effect in stabilizing EGFR mRNA by forming a circ_0053943/IGF2BP3/EGFR RNA-protein ternary complex, which finally promotes the proliferation and aggressiveness of UM cells. Overall, our finding may provide a new target, circ_0053943, for the diagnosis and treatment of UM.

Abbreviations

3'-UTR
3'- untranslated region
5'-UTR
5'- untranslated region

CCK-8
Cell counting kit- 8
CM
Conjunctival melanoma
EdU
5-Ethynyl-2'deoxyuridine
EGFR
epidermal growth factor receptor
circRNA
Circular RNA
FISH
Fluorescence in situ hybridization
GNA11
G protein subunit alpha 11
GNAQ
G protein subunit alpha Q
gDNA
Genomic DNA
HE
Hematoxylin and eosine
IGF2BP3
insulin-like growth factor 2 mRNA-binding protein 3
m^6A
N6-methyladenosine
MAPK
Mitogen activated protein kinase
MEK
MAPK/ERK kinase
METTL14
Methyltransferase-like 14
METTL3
Methyltransferase-like 3
miRNA
MicroRNA
mRNA
Messenger ribonucleic acid
qRT-PCR
Real-time quantification PCR
RasGRP3
RAS guanyl releasing protein 3

RIP
RNA-binding protein immunoprecipitation
RT-PCR
Reverse transcriptase PCR
siRNA
Small interfering RNA
UM
Uveal melanoma
WTAP
Wilms tumor associated protein

Declarations

Ethics approval and consent to participate

All experimental protocols were approved by the Ethics Committee of Nanjing Medical University and performed in accordance with the relevant guidelines and regulations. Written informed consents were obtained from all patients. All animal experiments were approved by the Institutional Animal Care and Use Committee of Nanjing Medical University (No. IACUC-2108017).

Consent for publication

Not applicable.

Availability of data and material

The datasets used and/or analyzed during the current study are available within the manuscript and its supplementary information files.

Competing interests

The authors declare that they have no competing interests.

Funding

This work is supported by the National Natural Science Foundation of China (Grant No.82171838), Provincial Science and Technology Department Social Development Plan (Grant No. BE2020722). The sponsor or funding organization had no role in the design or conduct of this research.

Authors' contributions

CXJ and LH conceived of the study and carried out its design. ZAD and WY performed the experiments. WZJ, ZXH, QS, QG, HZ, SSY and LL collected clinical samples. CXJ, ZAD, WY and WZJ conducted the

statistical analysis. ZAD wrote the paper and CXJ revised the paper. All authors read and approved the final manuscript.

Acknowledgments

We are grateful to all of the patients who participated in this study.

References

1. Chattopadhyay C, Kim DW, Gombos DS, Oba J, Qin Y, Williams MD, et al. Uveal melanoma: From diagnosis to treatment and the science in between. Cancer. 2016;122(15):2299 – 312.
2. Spagnolo F, Caltabiano G, Queirolo P. Uveal melanoma. Cancer treatment reviews. 2012;38(5):549 – 53.
3. Jager MJ, Shields CL, Cebulla CM, Abdel-Rahman MH, Grossniklaus HE, Stern MH, et al. Uveal melanoma. Nat Rev Dis Primers. 2020;6(1):2056-676X (Electronic).
4. Smit KN, Jager MJ, de Klein A, Kili E. Uveal melanoma: Towards a molecular understanding. Progress in retinal and eye research. 2020;75:100800.
5. Smit KN, van Poppelen NM, Vaarwater J, Verdijk R, van Marion R, Kalirai H, et al. Combined mutation and copy-number variation detection by targeted next-generation sequencing in uveal melanoma. Modern pathology: an official journal of the United States and Canadian Academy of Pathology, Inc. 2018;31(5):763 – 71.
6. Kristensen LA-O, Jakobsen T, Hager H, Kjems J. The emerging roles of circRNAs in cancer and oncology. Nat Rev Clin Oncol. 2021:1759–4782 (Electronic).
7. Goodall GJ, Wickramasinghe VA-O. RNA in cancer. Nat Rev Cancer. 2021;21(1):1474 – 768 (Electronic).
8. Zeng Z, Xia L, Fan S, Zheng J, Qin J, Fan X, et al. Circular RNA CircMAP3K5 Acts as a MicroRNA-22-3p Sponge to Promote Resolution of Intimal Hyperplasia Via TET2-Mediated Smooth Muscle Cell Differentiation. Circulation. 2020;143(4):1524–4539 (Electronic).
9. Schneider T, Bindereif A. Circular RNAs: Coding or noncoding? Cell Res. 2017 27(6):1748–7838 (Electronic).
10. Yang X, Li Y, Liu Y, Xu X, Wang Y, Yan Y, et al. Novel circular RNA expression profile of uveal melanoma revealed by microarray. Chinese Journal of Cancer Research. 2018;30(6):656 – 68.
11. Liu S, Chen L, Chen H, Xu K, Peng X, Zhang M. Circ_0119872 promotes uveal melanoma development by regulating the miR-622/G3BP1 axis and downstream signalling pathways. J Exp Clin Cancer Res. 2021;40(1):66.
12. He L, Li H, Wu A, Peng Y, Shu G, Yin GA-O. Functions of N6-methyladenosine and its role in cancer. Molecular cancer. 2019;18(1):1476–4598 (Electronic).
13. Wang X, Lu Z, Gomez A, Hon GC, Yue Y, Han D, et al. N6-methyladenosine-dependent regulation of messenger RNA stability. Nature. 2014;505(7481):1476–4687 (Electronic).

14. Lu H, Xie Y, Tran L, Lan J, Yang Y, Murugan NL, et al. Chemotherapy-induced S100A10 recruits KDM6A to facilitate OCT4-mediated breast cancer stemness. The Journal of clinical investigation. 2020;130(9):4607-23.
15. Huang H, Weng H, Sun W, Qin X, Shi H, Wu H, et al. Recognition of RNA N(6)-methyladenosine by IGF2BP proteins enhances mRNA stability and translation. Nature cell biology. 2018;20(3):1476–4679 (Electronic).
16. Paramasivam A, George R, Priyadharsini JV. Genomic and transcriptomic alterations in m6A regulatory genes are associated with tumorigenesis and poor prognosis in head and neck squamous cell carcinoma. Am J Cancer Res. 2021;11(7):2156–6976 (Print).
17. Xie F, Huang C, Liu F, Zhang H, Xiao X, Sun J, et al. CircPTPRA blocks the recognition of RNA N(6)-methyladenosine through interacting with IGF2BP1 to suppress bladder cancer progression. Molecular cancer. 2021;20(1):68.
18. Huang H, Weng H, Sun W, Qin X, Shi H, Wu H, et al. Recognition of RNA N(6)-methyladenosine by IGF2BP proteins enhances mRNA stability and translation. Nature cell biology. 2018;20(3):285 – 95.
19. Yu Y-Z, Lv D-J, Wang C, Song X-L, Xie T, Wang T, et al. Hsa_circ_0003258 promotes prostate cancer metastasis by complexing with IGF2BP3 and sponging miR-653-5p. Molecular cancer. 2022;21(1).
20. Glažar P, Papavasileiou P, Rajewsky N. circBase: a database for circular RNAs. RNA. 2014;20(11):1666-70.
21. Li Z, Peng Y, Li J, Chen Z, Chen F, Tu J, et al. N(6)-methyladenosine regulates glycolysis of cancer cells through PDK4. Nature communications. 2020;11(1):2578.
22. Chen RX, Chen X, Xia LP, Zhang JX, Pan ZZ, Ma XD, et al. N(6)-methyladenosine modification of circNSUN2 facilitates cytoplasmic export and stabilizes HMGA2 to promote colorectal liver metastasis. Nature communications. 2019;10(1):4695.
23. Tang Z, Kang B, Li C, Chen T, Zhang Z. GEPIA2: an enhanced web server for large-scale expression profiling and interactive analysis. Nucleic Acids Res. 2019;47(W1):W556-W560.
24. Rimoldi D, Salvi S, Liénard D, Lejeune FJ, Speiser D, Zografos L, et al. Lack of BRAF mutations in uveal melanoma. Cancer Research. 2003;63(18):5712-5.
25. Van Poppelen NM, Vaarwater J, Mudhar HS, Sisley K, Rennie IG, Rundle P, et al. Genetic background of iris melanomas and iris melanocytic tumors of uncertain malignant potential. Ophthalmology. 2018;125(6):904 – 12.
26. Yavuzyigitoglu S, Koopmans AE, Verdijk RM, Vaarwater J, Eussen B, Van Bodegom A, et al. Uveal melanomas with SF3B1 mutations: a distinct subclass associated with late-onset metastases. Ophthalmology. 2016;123(5):1118-28.
27. Vader M, Madigan M, Versluis M, Suleiman H, Gezgin G, Gruis NA, et al. GNAQ and GNA11 mutations and downstream YAP activation in choroidal nevi. British journal of cancer. 2017;117(6):884-7.
28. Chen X, Wu Q, Depeille P, Chen P, Thornton S, Kalirai H, et al. RasGRP3 Mediates MAPK Pathway Activation in GNAQ Mutant Uveal Melanoma. Cancer cell. 2017;31(5):685 – 96 e6.

29. Van Essen TH, van Pelt SI, Versluis M, Bronkhorst IH, Van Duinen SG, Marinkovic M, et al. Prognostic parameters in uveal melanoma and their association with BAP1 expression. British Journal of Ophthalmology. 2014;98(12):1738-43.
30. Martin M, Maßhöfer L, Temming P, Rahmann S, Metz C, Bornfeld N, et al. Exome sequencing identifies recurrent somatic mutations in EIF1AX and SF3B1 in uveal melanoma with disomy 3. Nature genetics. 2013;45(8):933-6.
31. Shain AA-O, Bagger MM, Yu R, Chang DA-O, Liu S, Vemula S, et al. The genetic evolution of metastatic uveal melanoma. Nat Genet. 2019;51(7):1546 – 718 (Electronic).
32. Chai P, Jia R, Li Y, Zhou C, Gu X, Yang L, et al. Regulation of epigenetic homeostasis in uveal melanoma and retinoblastoma. Progress in retinal and eye research. 2021:101030.
33. Zhang L, He X, Li F, Pan H, Huang X, Wen X, et al. The miR-181 family promotes cell cycle by targeting CTDSPL, a phosphatase-like tumor suppressor in uveal melanoma. J Exp Clin Cancer Res. 2018;37(1):1756–9966 (Electronic).
34. Li P, He J, Yang Z, Ge S, Zhang H, Zhong QA-OX, et al. ZNNT1 long noncoding RNA induces autophagy to inhibit tumorigenesis of uveal melanoma by regulating key autophagy gene expression. Autophagy. 2020;16(7):1554–8635 (Electronic).
35. Xing Y, Wen X, Ding X, Fan J, Chai P, Jia R, et al. CANT1 lncRNA Triggers Efficient Therapeutic Efficacy by Correcting Aberrant lncing Cascade in Malignant Uveal Melanoma. Molecular therapy: the journal of the American Society of Gene Therapy. 2017;25(5):1525-0024 (Electronic).
36. Peng C, Tan Y, Yang P, Jin K, Zhang C, Peng W, et al. Circ-GALNT16 restrains colorectal cancer progression by enhancing the SUMOylation of hnRNPK. Journal of experimental & clinical cancer research : CR. 2021;40(1):272.
37. Li B, Zhu L, Lu C, Wang C, Wang H, Jin H, et al. circNDUFB2 inhibits non-small cell lung cancer progression via destabilizing IGF2BPs and activating anti-tumor immunity. Nature communications. 2021;12(1):295.
38. Lin S, Choe J, Du P, Triboulet R, Gregory RI. The m(6)A Methyltransferase METTL3 Promotes Translation in Human Cancer Cells. Molecular cell. 2016;62(3):335 – 45.
39. He L, Li H, Wu A, Peng Y, Shu G, Yin G. Functions of N6-methyladenosine and its role in cancer. Molecular cancer. 2019;18(1):176.
40. Tang J, Wan Q, Lu J. The prognostic values of m6A RNA methylation regulators in uveal melanoma. BMC cancer. 2020;20(1):674.
41. Jia R, Chai P, Wang S, Sun B, Xu Y, Yang Y, et al. m(6)A modification suppresses ocular melanoma through modulating HINT2 mRNA translation. Molecular cancer. 2019;18(1):161.
42. Wan Q, Tang J. Exploration of potential key pathways and genes in multiple ocular cancers through bioinformatics analysis. Graefes Arch Clin Exp Ophthalmol. 2019;257(10):2329-41.
43. Fang R, Chen X, Zhang S, Shi H, Ye Y, Shi H, et al. EGFR/SRC/ERK-stabilized YTHDF2 promotes cholesterol dysregulation and invasive growth of glioblastoma. Nature communications. 2021;12(1):177.

44. Hino N, Rossetti L, Marin-Llaurado A, Aoki K, Trepat X, Matsuda M, et al. ERK-Mediated Mechanochemical Waves Direct Collective Cell Polarization. Developmental cell. 2020;53(6):646 – 60 e8.
45. Ma G, Liang Y, Chen Y, Wang L, Li D, Liang Z, et al. Glutamine Deprivation Induces PD-L1 Expression via Activation of EGFR/ERK/c-Jun Signaling in Renal Cancer. Molecular cancer research: MCR. 2020;18(2):324 – 39.
46. Tiemin P, Fanzheng M, Peng X, Jihua H, Ruipeng S, Yaliang L, et al. MUC13 promotes intrahepatic cholangiocarcinoma progression via EGFR/PI3K/AKT pathways. Journal of hepatology. 2020;72(4):761 – 73.
47. Zhangyuan G, Wang F, Zhang H, Jiang R, Tao X, Yu D, et al. VersicanV1 promotes proliferation and metastasis of hepatocellular carcinoma through the activation of EGFR-PI3K-AKT pathway. Oncogene. 2020;39(6):1213-30.
48. Topcu-Yilmaz P, Kiratli H, Saglam A, Soylemezoglu F, Hascelik G. Correlation of clinicopathological parameters with HGF, c-Met, EGFR, and IGF-1R expression in uveal melanoma. Melanoma research. 2010;20(2):126 – 32.
49. Amaro A, Mirisola V, Angelini G, Musso A, Tosetti F, Esposito AI, et al. Evidence of epidermal growth factor receptor expression in uveal melanoma: inhibition of epidermal growth factor-mediated signalling by Gefitinib and Cetuximab triggered antibody-dependent cellular cytotoxicity. European journal of cancer. 2013;49(15):3353-65.
50. Hurks HM, Metzelaar-Blok JA, Barthen ER, et al. Expression of epidermal growth factor receptor: risk factor in uveal melanoma. Invest Ophthalmol Vis Sci. 2000;41(8):2023–2027.
51. Gu Y, Niu S, Wang Y, Duan L, Pan Y, Tong Z, et al. DMDRMR-Mediated Regulation of m6A-Modified CDK4 by m6A Reader IGF2BP3 Drives ccRCC Progression. Cancer Research. 2021;81(4):923 – 34.
52. Chen X, Wu Q, Tan L, Porter D, Jager MJ, Emery C, et al. Combined PKC and MEK inhibition in uveal melanoma with GNAQ and GNA11 mutations. Oncogene. 2014;33(39):4724-34.

Figures

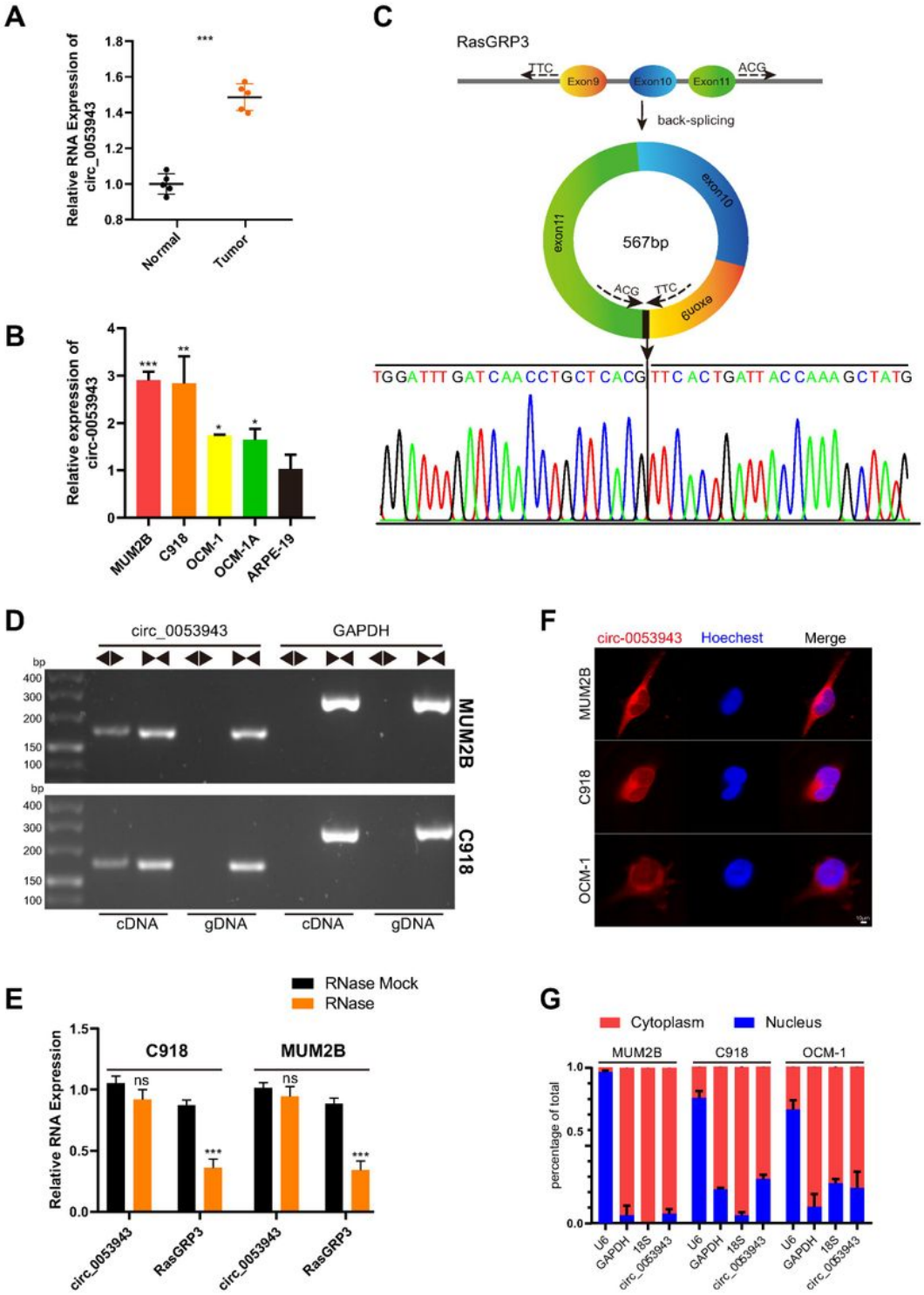

Figure 1

The characterization of circ_0053943 in UM. A. The expression of hsa_circ_0053943 in 5 ocular melanoma tissues and 5 human normal melanocyte tissues in our cohort. **B.** The schematic illustration showed the back splicing of circ_0053943, and the sanger sequence validated the splicing site. **C.** The expression level of circ_0053943 in ARPE-19 cells and 4 UM cell lines (MUM2B, C918, OCM-1, OCM-1A). **D.** PCR and agarose gel electrophoresis confirmed the circular formation of circ_0053943, using divergent

and convergent primers in gDNA and cDNA of MUM2B and C918 cells. GAPDH was used as a negative control. **E.** Circ_0053943 and linear RasGRP3 expression levels were detected after RNase R in MUM2B and C918. **F, G.** FISH and subcellular fractionation assays indicated that circ_0053943 was predominately localized in the cytoplasm of UM cells. $^{ns}p > 0.05$, $*p < 0.05$, $**p < 0.01$, $***p < 0.001$.

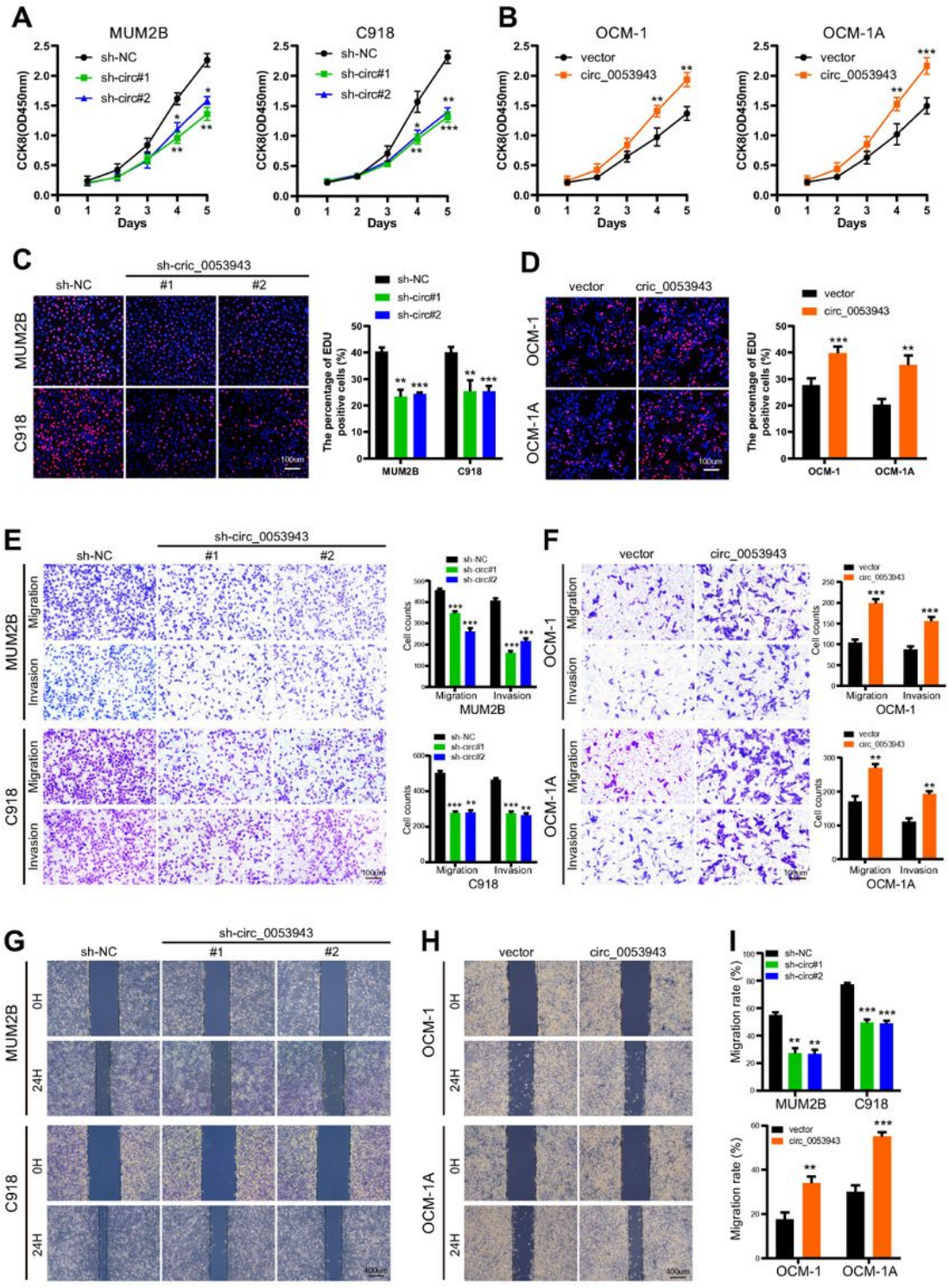

Figure 2

Circ_0053943 promotes the proliferation, migration, and invasion of UM cells in vitro. A, B. CCK8 assays were applied to determine the growth curves of circ_0053943 knockdown or overexpression cells. **C, D.** EdU assays were performed to assess the cell proliferation ability. **E, F.** Transwell migration and invasion assays were applied to evaluate the migration and invasion abilities of UM cells. **G, H.** Cell migration ability was assessed by wound healing assay. *$p < 0.05$, **$p < 0.01$, ***$p < 0.001$.

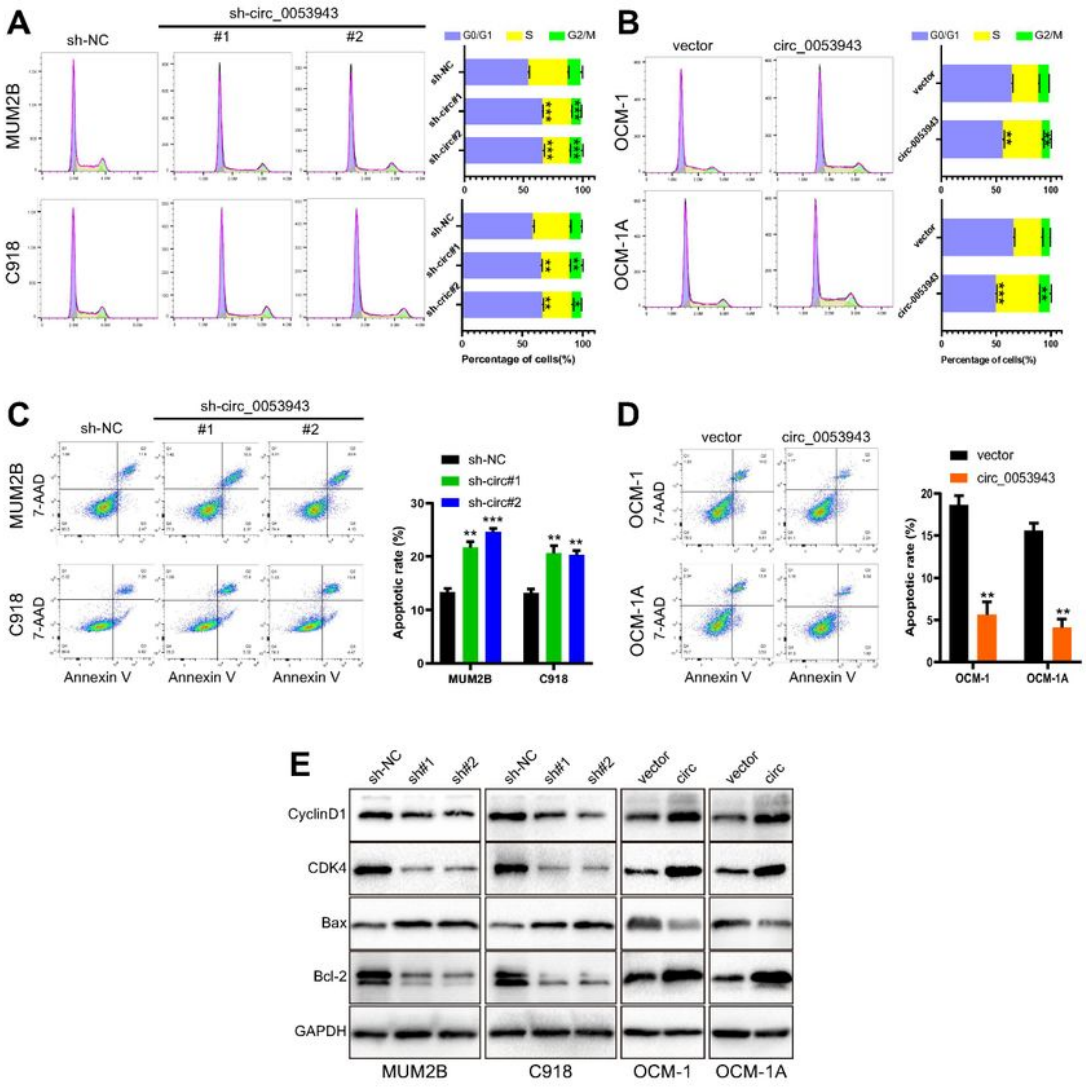

Figure 3

Circ_0053943 regulates the cell cycle and apoptosis of UM cells. A, B. Cell cycle distributions were detected by flow cytometry in circ_0053943 knockdown or overexpression cells. **C, D.** The apoptotic rates were performed and analyzed after cells were treated with 0.5 mM H_2O_2 for 4 h. All data are presented as the means ± SD of three independent experiments. **E.** The expression of cell cycle and apoptosis makers (Cyclin D1, CDK4, Bcl-2, and Bax) were detected by western blot in relatively treated cells. **$p < 0.01$, ***$p < 0.001$.

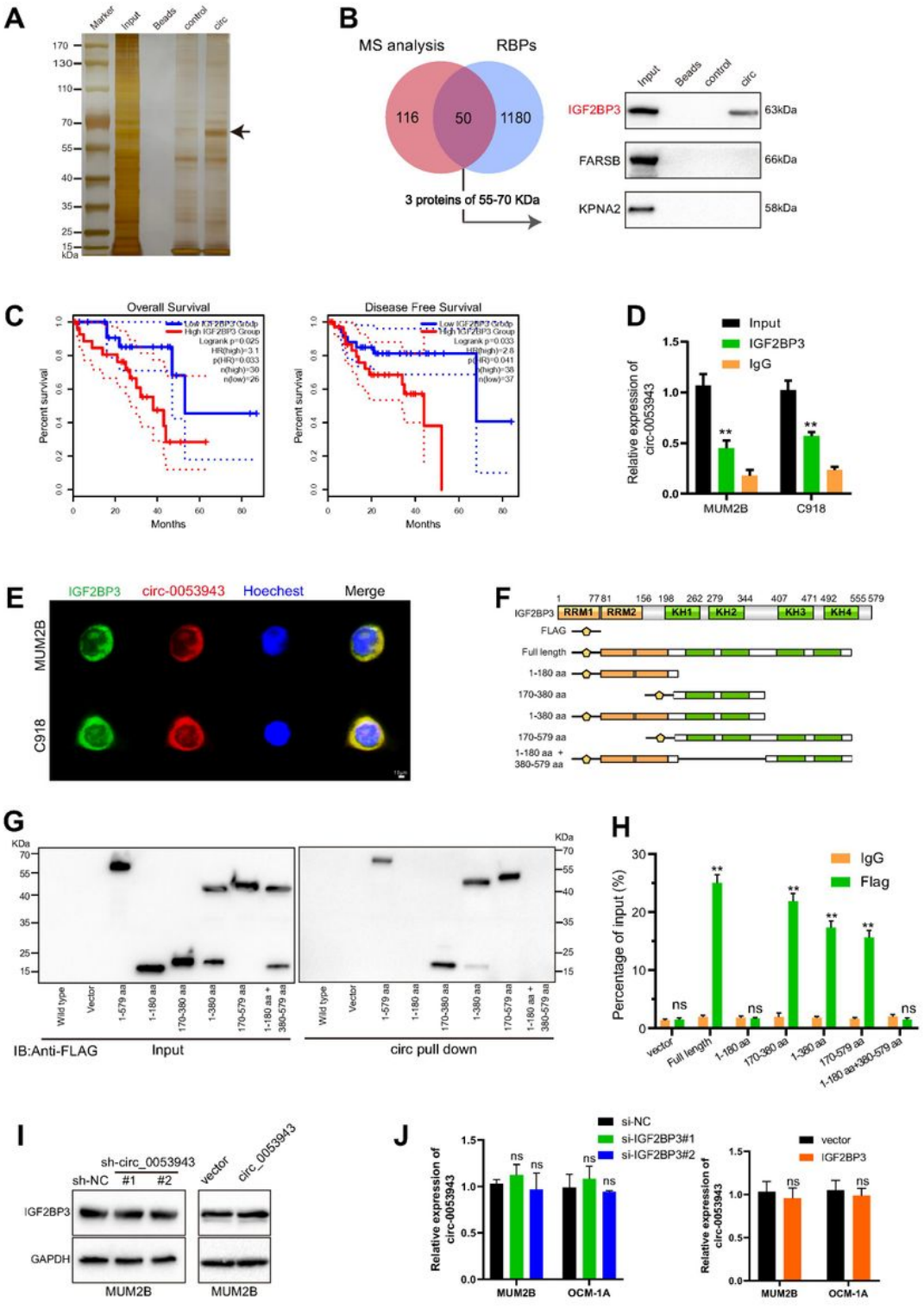

Figure 4

Circ_0053943 binds to the KH1 and KH2 domains of IGF2BP3. A-C. RNA pulldown assay followed by silver staining, western blot, and RIP assay indicated that circ_0053943 specifically interacted with IGF2BP3. **D.** Kaplan-Meier plots of the overall survival (OS) and disease-free survival (DFS) of UM patients with high and low levels of IGF2BP3 according to the Cancer Genome Atlas (TCGA) data. **E.** Dual RNA FISH and immunofluorescence assays showed that circ_0053943 and IGF2BP3 colocalized in the cytoplasm of MUM2B and C918. **F.** Functional domain and truncated mutation annotation of IGF2BP3. **G, H.** RIP assay and RNA pulldown assay confirmed that circ_0053943 characteristically interacted with the KH1 and KH2 domains of IGF2BP3. **I.** The protein level of IGF2BP3 in circ_0053943 knockdown and overexpression cells. **J.** The circ_0053943 expression level in IGF2BP3 silencing and upregulated cells. $^{ns}p > 0.05$, $^{*}p < 0.05$, $^{**}p < 0.01$, $^{***}p < 0.001$.

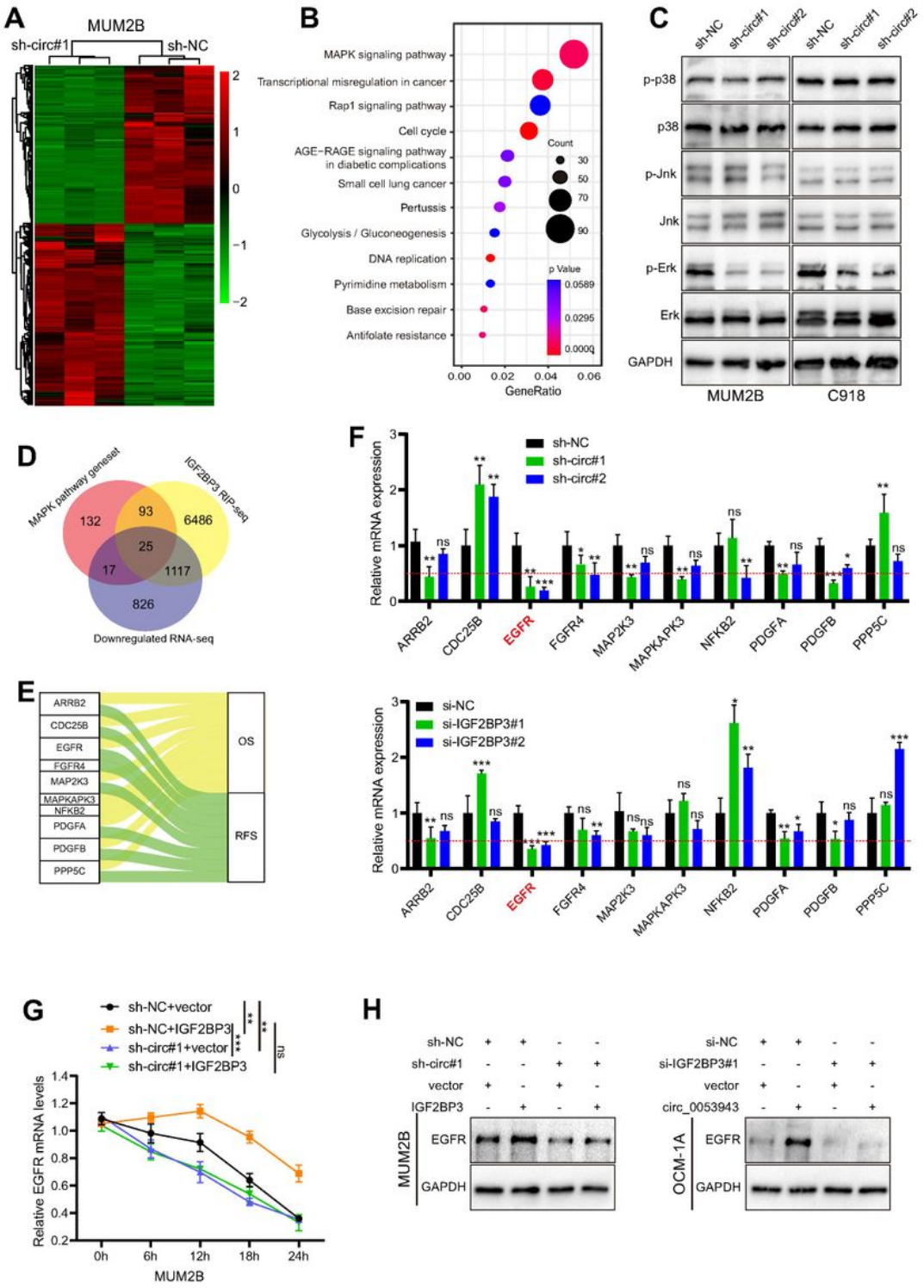

Figure 5

EGFR is downregulated by circ_0053943 and has a connection with UM progression. A. Heatmap showed the RNA-seq result in circ_0053943 knockdown and control MUM2B cells. **B.** The top 12 enriched KEGG terms for differentially expressed genes (DEGs). The color intensities represent the *P* values. The circle sizes represent the counts of DEGs. **C.** Western blot indicated total and phosphorylated proteins of MAPK signaling pathway. **D.** Venn diagram showing the 25 overlapping genes by downregulated genes of

silencing circ_0053943 RNA-sequence data and MAPK pathway gene set together with IGF2BP3 binding genes of IGF2BP3 RIP-sequence data (GSE90642 and GSE90639). **E.** Sankey diagram representing 10 overlapping genes associated with UM progression. **F.** qRT-PCR analysis of the 10 overlapping genes transcript levels in the circ_0053943 knockdown (upper) and IGF2BP3 knockdown (down) MUM2B cells. **G.** The half-life of EGFR mRNA after treatment with 5 μM actinomycin D for the indicated times in the silencing circ_0053943 cells with ectopically expressed IGF2BP3. **H.** The protein levels of EGFR in circ_0053943 knockdown cells with ectopically expressed IGF2BP3(left), and IGF2BP3 knockdown cells with ectopically expressed circ_0053943 cells (right). All data are presented as the means ± SD of three independent experiments. $^{ns}p > 0.05$, $*p < 0.05$, $**p < 0.01$, $***p < 0.001$.

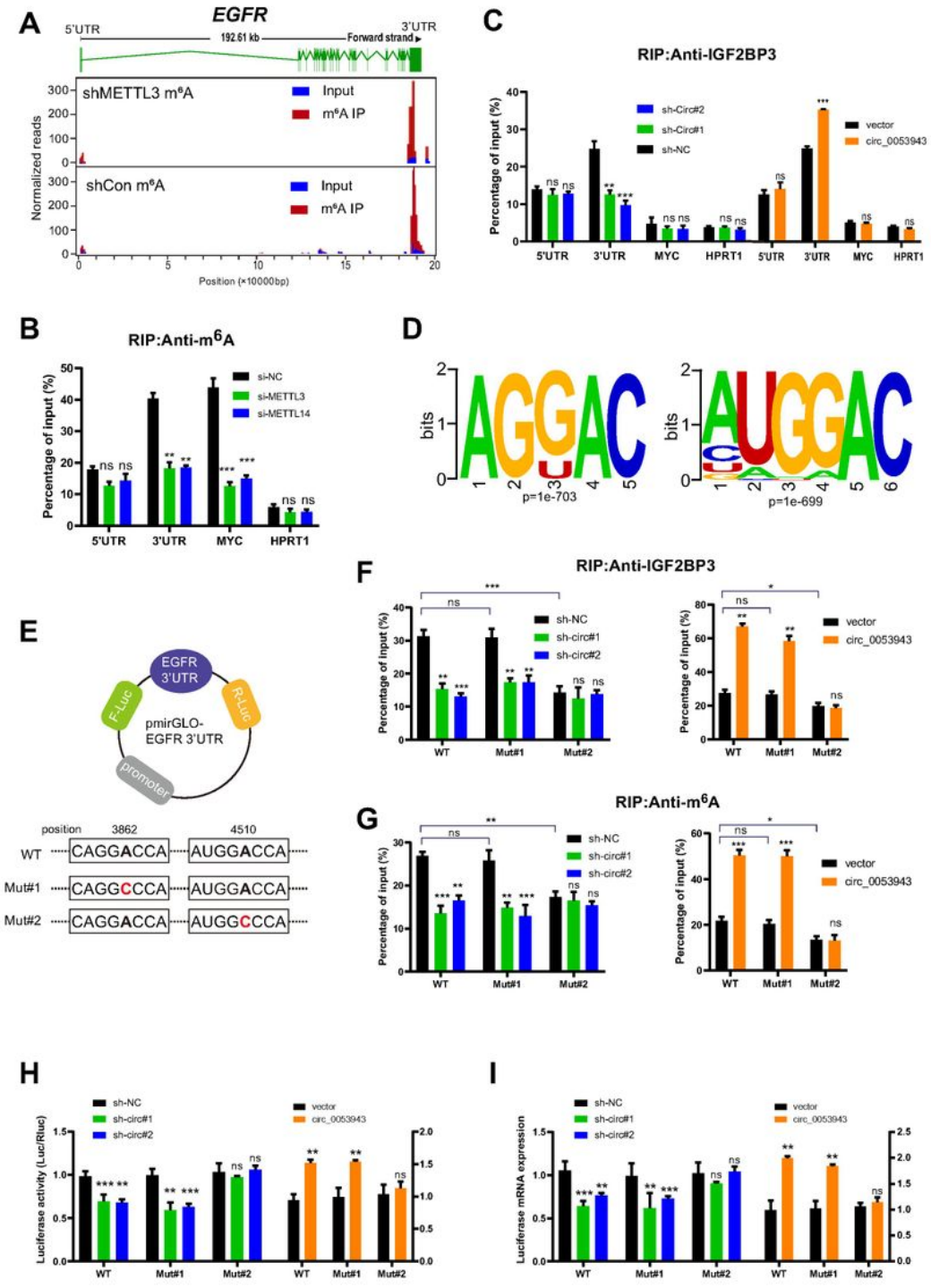

Figure 6

Circ_0053943 cooperates with IGF2BP3 to regulate EGFR in an m6A-dependent manner. A. Distribution of m6A peaks across the EGFR transcript based on m6A RIP-sequence data. **B.** RIP qRT-PCR showing the enrichment of m6A modification in the EGFR 5' UTR /3' UTR regions in the METTL3 and METTL14 knockdown MUM2B cells. MYC CRD was used as a positive control. HPRT1 was used as a negative control. **C.** RIP qRT-PCR detecting the enrichment of IGF2BP3 in the EGFR 3'UTR, 5'UTR, MYC CRD, and

HPRT1 in circ_0053943 knockdown and overexpressed cells. **D.** Two top consensus sequences of IGF2BP3-binding sites and the m6A motif detected by SRAMPA and RMBase V2.0 motif analysis. **E.** Schematic representation of wild-type (WT) and mutated (MUT) EGFR 3'UTR of the pmirGLO vector. **F, G.** RIP qRT-PCR detection of the enrichment of IGF2BP3 and m^6A in the EGFR 3'UTR WT and MUT luciferase reporters in the circ_0053943 knockdown and overexpression cells. **H, I.** Relative luciferase activity and luciferase mRNA expression of the luciferase reporter gene with EGFR 3'UTR WT and MUT reporters in control and circ_0053943 knockdown or overexpression MUM2B cells. All data are presented as the means ± SD of three independent experiments. $^{ns}p > 0.05$, $^{*}p < 0.05$, $^{**}p < 0.01$, $^{***}p < 0.001$.

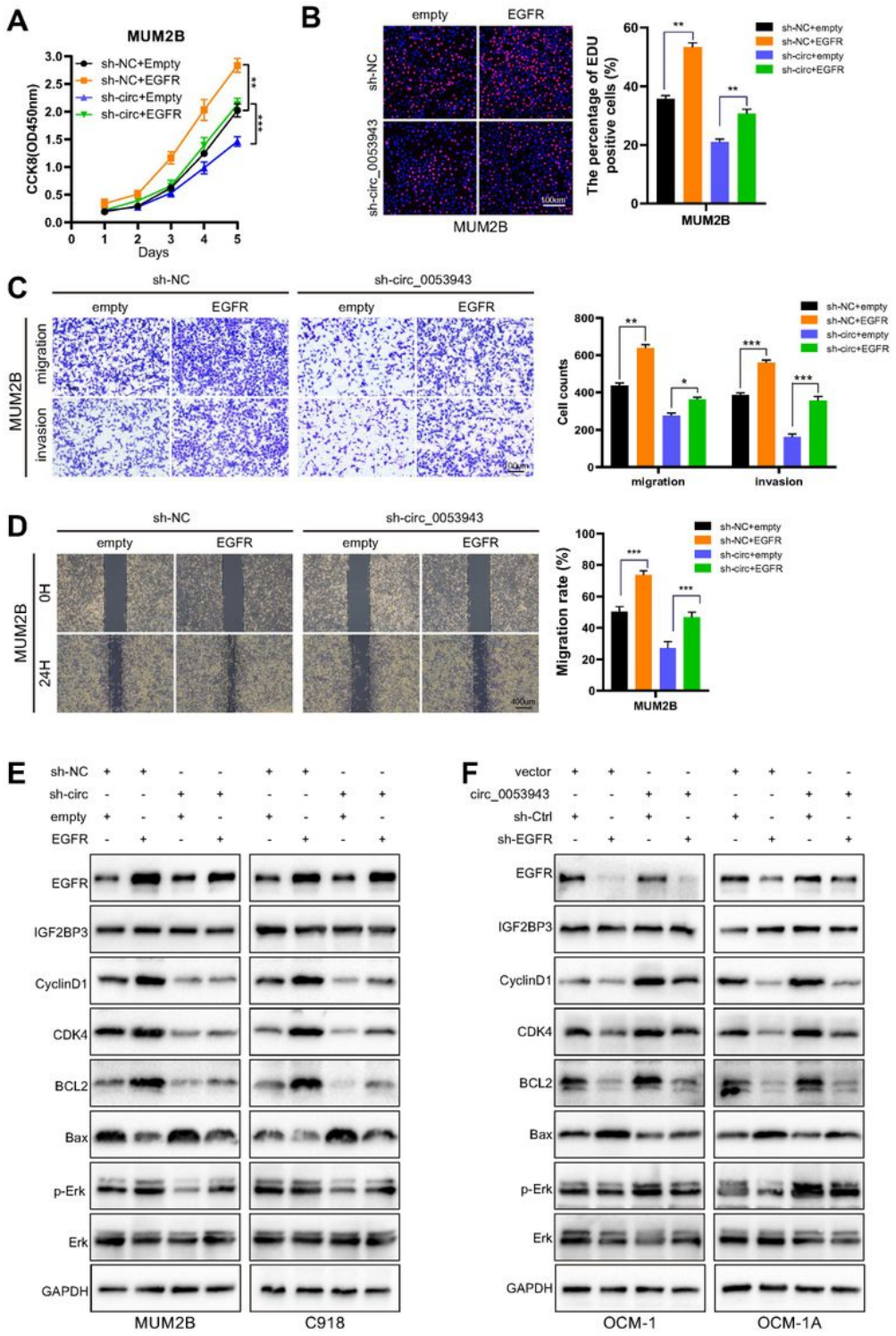

Figure 7

Circ_0053943 regulates UM proliferation, metastasis, cell cycle, and apoptosis via upregulating EGFR expression in vitro. A, B. CCK8 and EdU were used to detect UM cell proliferation ability in circ_0053943 knockdown cells with ectopically expressed EGFR. **C, D.** Transwell and wound healing assays detected UM cell metastasis capacity in circ_0053943 knockdown cells with ectopically expressed EGFR. **E, F.** The expression of cell cycle and apoptosis makers (Cyclin D1, CDK4, Bcl-2, and Bax) along with EGFR,

IGF2BP3, Erk, and p-Erk were detected by western blot in relatively treated cells. All data are presented as the means ± SD of three independent experiments. *$p < 0.05$, **$p < 0.01$, ***$p < 0.001$.

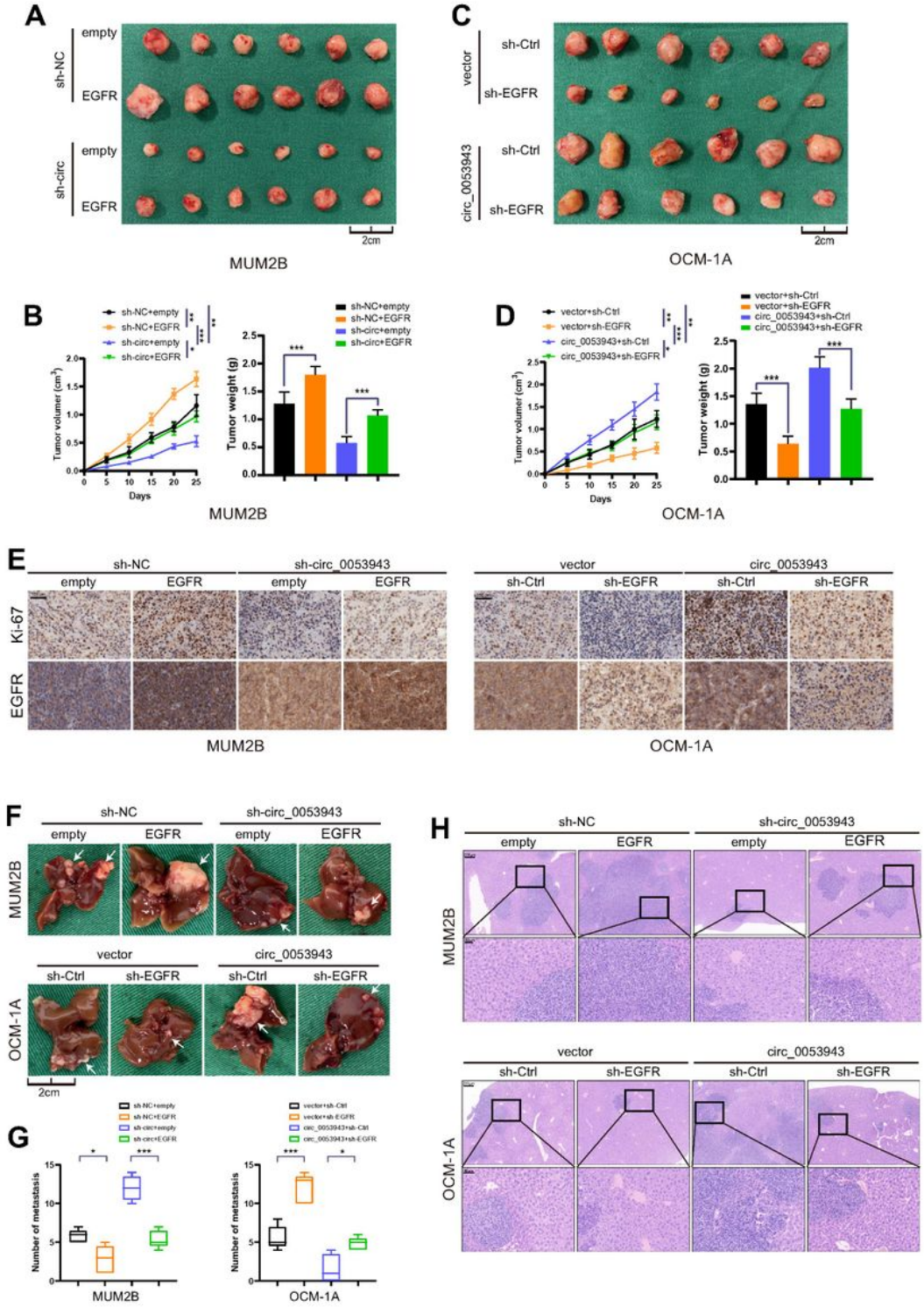

Figure 8

Circ_0053943 promotes UM proliferation and metastasis via upregulating EGFR expression in vivo. A, B. Representative photographs of subcutaneous xenograft tumors were obtained from the different groups

of nude mice transfected MUM2B cells with knockdown circ_0053943 and ectopically expressed EGFR. Tumors were observed by tumor size and average weight. **C, D.** Representative photographs of subcutaneous xenograft tumors were obtained from the different groups of nude mice transfected OCM-1A cells with knockdown EGFR and ectopically expressed circ_0053943. Tumors were observed by tumor size and average weight. **E.** Protein levels of Ki-67 and EGFR in the tumor samples were determined by IHC. **F-H.** Representative photographs and HE staining of liver metastases were obtained from nude mice transfected with relatively treated cells, and the number of metastases was measured. All data are presented as the means ± SD of three independent experiments. *$p < 0.05$, **$p < 0.01$, ***$p < 0.001$.

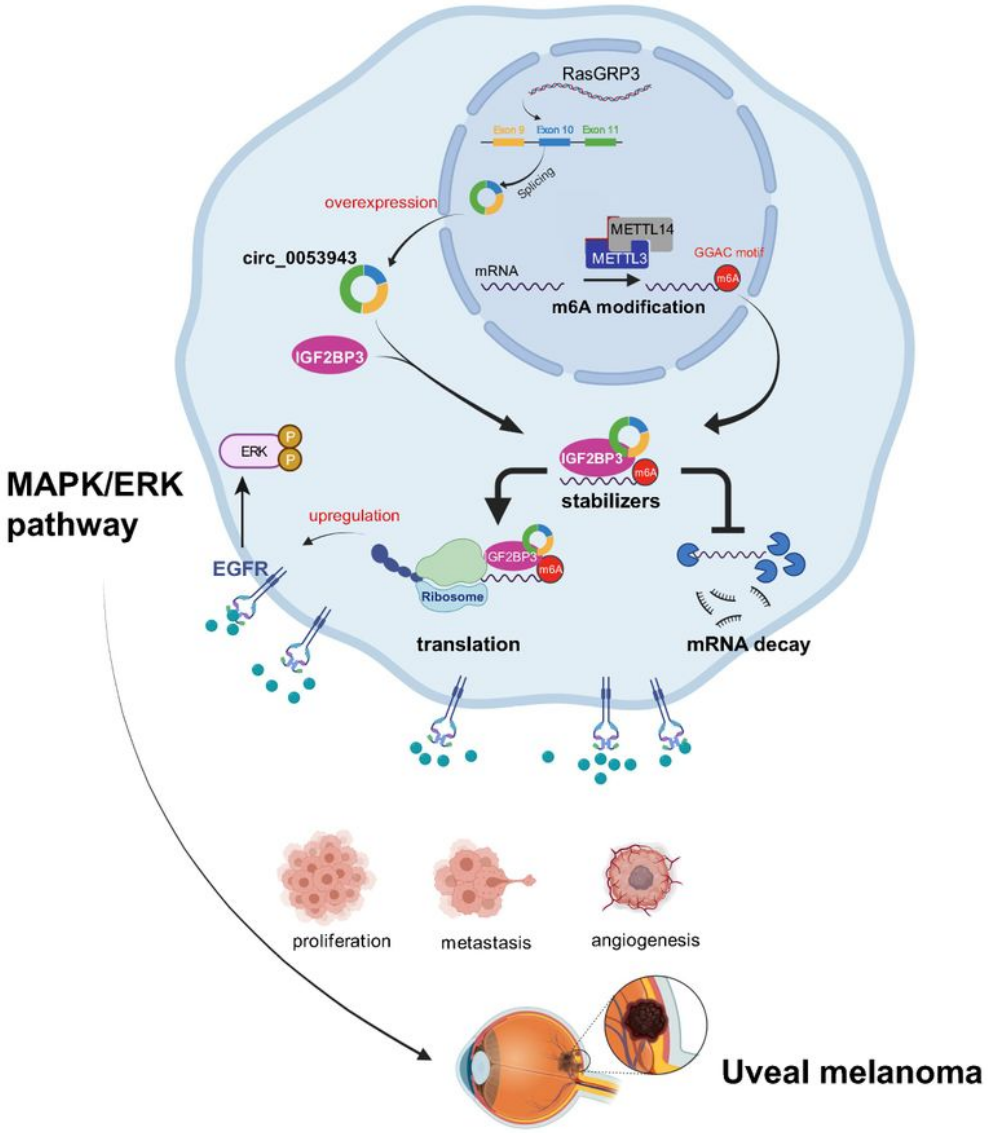

Figure 9

A schematic model for the mechanisms of circ_0053943 in UM.

Supplementary Files

This is a list of supplementary files associated with this preprint. Click to download.

- figS1.pdf
- figS2.pdf
- figS3.pdf
- figS4.pdf
- figS5.pdf
- figS6.pdf
- figS7.pdf
- supplementaltable1.xlsx
- supplementaltable2.xlsx
- supplementaltable3.xlsx
- supplementaltable4.xlsx
- supplementaltable5.xlsx
- supplementaltable6.xlsx
- supplementaltable7.xlsx